

Mechanochemical synthesis and characterization of pure Co₂B nanocrystals

MUSTAFA BARIS^{1,*}, TUNCAY SIMSEK² and ADNAN AKKURT³

¹Eti Maden Works General Management, Ankara 06105, Turkey

²Department of Physics Engineering, Hacettepe University, Ankara 06800, Turkey

³Department of Industrial Design Engineering, Gazi University, Ankara 06500, Turkey

MS received 5 January 2016; accepted 2 February 2016

Abstract. Cobalt boride (Co₂B) is a significant transition metal boride having a wide range of usage area due to its high oxidation, abrasion and corrosion resistance as well as its superior electrochemical, magnetic and anisotropic properties. In this study, pure Co₂B nanocrystals were synthesized with Co, B₂O₃ and Mg as starting materials via the mechanochemical synthesis (MCS) method by high-energy planetary ball mill in a hardened steel vial with hardened steel balls. All the experiments were conducted under Ar atmosphere at different rotational speeds and at 20 : 1–30 : 1–40 : 1 ball-to-powder ratios. Leaching of Co₂B + MgO powder mixtures occurred after milling and purified with acetic acid and pure Co₂B nanocrystals were obtained in solid form. The Co₂Bs were characterized through X-ray diffraction, scanning electron microscopy, vibrating sample magnetometer, Brunauer–Emmett–Teller and specific density analyses, and effects of synthesis parameters on product properties were revealed. Surface areas of the powders synthesized at 40 : 1 ball-to-powder ratio at different rotational speeds were measured as 21.14, 40.36 and 52.33 m² g⁻¹, respectively. Crystallite sizes of Co₂B nanocrystals were between 7.27 and 9.84 nm and their specific density varied between 7.61 and 7.78 g cm⁻³. It was determined that all samples were saturated and exhibited hysteresis and ferromagnetic behaviours, and saturation magnetization was between 35 and 50 emu g⁻¹.

Keywords. Cobalt boride; mechanochemical synthesis; transition metals; ball milling; nanocrystals.

1. Introduction

Cobalt boride (Co₂B) was first introduced as a hetero- gen catalyst in 1969 [1]. The role of Co₂B in hydro- gen production was better understood by Maybury *et al* [2]. A binary boride catalyst including both cobalt and nickel borides was also developed [3]. The hydrogenation activity of Co₂B was investigated by Chen and Wu [4] in 1991. The solvothermal production method for Co₂B nanoparticles was first proposed by Glavee *et al* [5] in 1993. A synthesis protocol was proposed for controlling the size and properties of Co₂B nanoparticles by Petit and Pileni [6] in 1997. Co₂B nanoparticles have been com- monly employed as effective catalysts both for the hydro- genation and hydrogen production processes [7–17]. A study on the hydrogenation activity of Co₂B particles in the CTAB/ 1-hexanol/water reversed micellar system was performed by Ma *et al* [7]. Co₂B was first tried as a catalyst for hydro- gen generation from alkaline NaBH₄ solution [9]. In the fol- lowing years, various studies were conducted on the hydro- gen production using only Co₂B or binary systems includ- ing Co₂B together with nickel or iron boride [10–17]. In all these studies, Co₂B nanoparticles produced by solvothermal procedure were tried as catalyst.

Beyond the solvothermal synthesis method, Co₂B was also synthesized by Kanomata *et al* [18] via the thermal method in 1997 and by Choi *et al* [19] via the thermal plasma method in 2014. Although many studies for synthesis of metal borides by the mechanochemical synthesis (MCS) method have been done [20–36], only one study was performed for synthe- sis of Co₂B by Wang *et al* [37] published in 2012. By considering the gap in the literature, a newly developed mechanochemical synthesis protocol for the synthesis of Co₂B nanoparticles was proposed. The synthesis method, size distribution, morphology and structural properties of the Co₂B nanoparticles obtained by the mechanochemical synthesis are presented in detail in this paper.

2. Material and methods

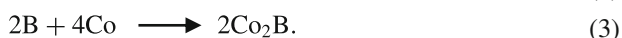
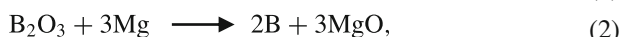
2.1 Material

Co (173 μm, ≥99.90%, Sigma Aldrich), Mg (138 μm, ≥99.00%, Sigma Aldrich) and B₂O₃ (598 μm, ≥98.00%, Eti Mine) were used as the starting materials in the experiments. All experiments were carried out under Argon (99.99%) atmosphere. Synthesis experiments were performed with a hardened steel vial and 3 mm × 15 mm diameter hardened steel balls. Purification process was performed in the 0.1 M acetic acid (AA–CH₃COOH) solution.

* Author for correspondence (mustafabaris@etimaden.gov.tr)

2.2 Mechanochemical synthesis

Synthesis experiments were performed in 3 stages: preparation of starting powders, high-energy ball milling and purification. Starting powders grain size distributions were determined in Malvern Mastersizer-2000 laser grain size device and optical microscope images were taken in Leica M-205C optical microscope. Before milling process, the starting powders were weighed by using precision balance at the ratio of 4 : 1 : 3.3 mol, in such a way that Mg was more than 10%, according to equations (1–3) and were placed with balls into hardened steel vial. The vial was isolated by being closed with double-valve inert atmospheric cap. High-purity Ar gas was fed at 20 ml min⁻¹ flow speed from inlet valve for 30 min to provide the inert atmosphere in the internal volume of vial and gas discharge was taken from outlet valve. Gas flow was stopped by closing inlet and outlet valves at the end of time and the milling processes were performed by placing the prepared vial into mill



The milling processes were carried out by using Fritsch P6 high-energy planetary ball mill which has a transmission ratio of 1 : -1.82 between planetary disk and grinding bowl. Rotational speed was kept constant at 300 rpm to determine the diameter of balls to be used in experiments that are performed and based on rotational speed of the main plate. Ball-to-powder ratio (BPR), rotational speed and milling time were taken as variable parameters in the synthesis experiments according to results of preliminary tests. Powder mixtures, prepared at 20 : 1–30 : 1–40 : 1 BPR according to three balls with a 15 mm diameter, were milled at 250–300–350 rotational speeds for different times up to 60 h. Table 1 shows details of preliminary tests and synthesis experiments.

2.3 Characterization of nanocrystals

Crystal structures of nanoparticles were analysed by X-ray diffraction (XRD) spectrophotometer (Rigaku D/MAX-2200) at 4° min⁻¹ scanning rate and in the angle range of 20–90° (2θ).

PDF 2000 library was used in JADE 7 analysis software for identification of graphics obtained as a result of the analysis. Powders were leached by using a magnetic stirrer for purification at the ratio of 1/250 g ml⁻¹ within 0.1 M acetic acid (AA-CH₃COOH) solution for 30 min at 250 rpm rotational speed. Solid–liquid separation was performed by centrifuging solutions (Heraeus Labofuge-Ae) at 3000 rpm rotational speed for 5 min after the leaching process. Then, the particles were washed with distilled water–ethanol, and dried for a day at 70°C under a vacuum of 20 mbar (Memmert VO-400).

The nanocrystals morphology was determined via scanning electron microscopy (SEM) (FEI Quanta-200F). While magnetic properties of powders obtained at different rotational speeds were determined by vibrating sample magnetometer (VSM, Quantum Design PPMS P525) at 25°C within ± 20 kOe magnetic field ranges, their surface areas were determined by a surface area and pore-size analyzer (Quantochrome Nova 220E) using nitrogen adsorption–desorption method together with Brunauer–Emmett–Teller (BET) equation, and their specific densities were specified in the helium pycnometer (Micromeritics AccuPyc-II).

3. Results and discussion

The *d*(0.5) grain size was determined, respectively, 173, 138 and 598 μm as a result of laser grain size analysis of Co, Mg and B₂O₃, which were used as the starting materials. It was detected from SEM images that Co particles were spherical, Mg particles were in irregular flat form and B₂O₃ particles were in irregular form of spherical. If the grain size of the starting materials in the MCS is smaller than 200 μm, then it is a preferred situation. However, the grain size can be chosen larger provided that it is smaller than the diameter of balls [38]. Figure 1 shows SEM images and grain size distribution graphics of the used chemicals.

Various parameters should be under control in the MCS. These parameters, which varied depending on the type of mill used and grain sizes of the starting powders, ball diameter, number of balls, BPR, rotational speed and vial fill rate, had significant effects on phase, microstructure and properties of final product. It is essential for these parameters to be

Table 1. Details of preliminary tests and synthesis experiments.

Amount of initial powders (g)	Diameter of balls (mm)	Number of balls	Ball-to-powder ratio (BPR)	Rotation (RPM)	Time (h)
<i>Preliminary tests</i>					
2.10	5	82	20 : 1	300	30
2.10	10	10	20 : 1	300	30
2.10	15	3	20 : 1	300	30
4.30	15	3	10 : 1	300	30
<i>Synthesis experiments</i>					
2.10	15	3	20 : 1	250	10, 20
1.40			30 : 1	300	30, 40
1.05			40 : 1	350	50, 60

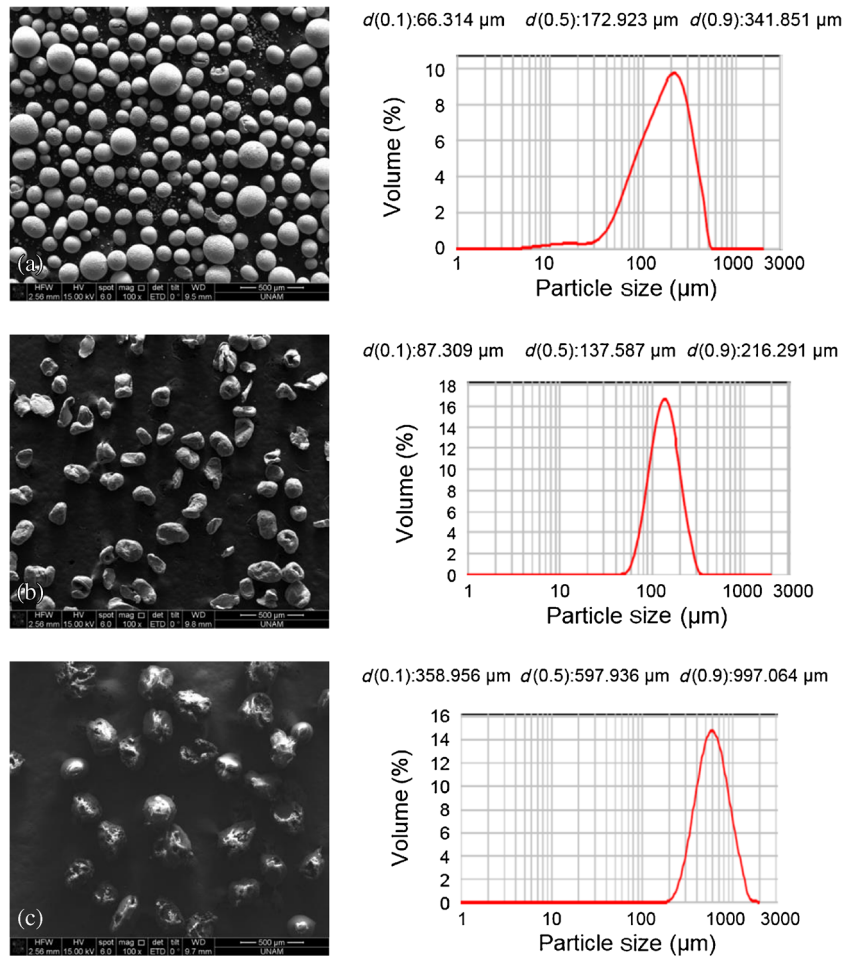


Figure 1. SEM images and grain size distributions of the starting materials: (a) Co, (b) Mg and (c) B_2O_3 .

within critical limits for the desired reaction to be carried out successfully in the vial used.

Especially, it is very important to choose the speed of mill which directly affects the synthesis period and forms the source of mechanical energy, within the correct range based on the type of mill. In the planetary-type mills, kinetic energy ($E_k = 1/2mv^2$, m , mass, v , velocity) released during the milling is directly proportional to the square of rotational speed and increase in the rotational speed ensures the increase of kinetic energy applied to the milled powders in the environment. However, the fact that rotational speed exceeds critical limit enables the balls in the environment to adhere to the walls of vial and the reaction does not occur in an environment without collision. In addition, energy released by the increase of rotational speed causes an increase in the ambient temperature and a contamination arising from vial and balls. While the increase of ambient temperature provides advantages for some reactions, it is an undesirable situation for some reactions. Hence, contamination is not a desired situation [38].

In addition to the rotational speed which directly affects kinetic energy, diameter of the ball used in the milling is also

directly proportional to kinetic energy formed. When the bigger balls used, the mass of balls and the energy formed will also increase. However, to determine the sizes, for which free collision required for the reaction could not be prevented in the preference of the ball diameter. Thus, based on studies in the literature [26,27,39,40], the rotational speed was fixed at 300 rpm and the milling was performed with 5–10–15 mm diameter balls in 20 : 1 and 10 : 1 BPR for 30 h each to determine optimum ball diameter and rotational speed with preliminary tests before synthesis experiments. Figure 2 shows XRD analysis of powders obtained at the end of milling on preliminary tests.

XRD graphic in figure 2 that shows Co, B_2O_3 and Mg, which were used as starting materials were existed till the end of 30 h milling performed by using 5 mm (a) and 10 mm (b) diameter balls at 20 : 1 BPR and it was determined that the reaction did not start. As the diameter of balls was increased to 15 mm, the reaction started at both 20 : 1 (c) and 10 : 1 (d) BPR and the reaction progressed faster at 20 : 1 BPR. Similarly, in the NbB_2 synthesis study conducted by Iizumi *et al* [24] in the planetary high-energy ball mill based on their elements, they determined that the reaction was completed at 20 : 1 BPR within 50 h by using 5 mm diameter balls

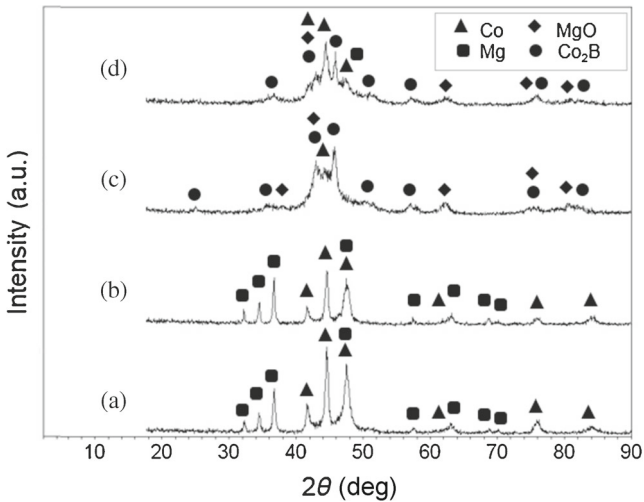


Figure 2. XRD graphic of final powders obtained from preliminary tests: (a) \emptyset 5 mm-20 : 1 BPR, (b) \emptyset 10 mm-20 : 1 BPR, (c) \emptyset 15 mm-20 : 1 BPR and (d) \emptyset 15 mm-10 : 1 BPR.

and within 20 h by using 16 mm diameter balls. According to preliminary tests and results obtained from literature, it was decided to carry out the synthesis experiments at 20 : 1–30 : 1–40 : 1 BPR and 250–300–350 rpm rotational speeds by using three balls with a 15 mm diameter and the milling processes were performed up to 60 h.

To synthesize by the MCS method, enough space should be available in the milling media. Synthesizing occurs mainly due to impact forces exerted on powder particles via balls. Therefore, the vial filling rate (VFR) must be chosen perfectly [38]. VFRs were calculated according to equation (4) by considering volumes of starting materials and the balls used. In the equation, V_v represents vial volume, V_p represents volume of starting materials used and V_b represents volume of the balls used. The balls in the environment have to freely collide with each other and with the wall of vial to achieve maximum energy during the milling process. It is beneficial that for free collision, VFR should be as low as possible depending on other milling parameters. According to calculations, VFR ranged between 6.54 and 7.34% in the synthesis experiments

$$\text{VFR} = \frac{V_p + V_b}{V_v}, \quad (4)$$

$$V_p = V_{\text{Co}} + V_{\text{B}_2\text{O}_3} + V_{\text{Mg}}, \quad (5)$$

$$V_b = 4/3\pi r^3. \quad (6)$$

Amount of powder lost as a result of adhesion to vial and balls was determined by weighing all samples, which were taken from vial after milling processes, with precision balance. Powders obtained after milling from continuously performed synthesis experiments were taken from vial with the help of a brush and the powder losses were detected based on the initial amount. It was found that the powder losses varied

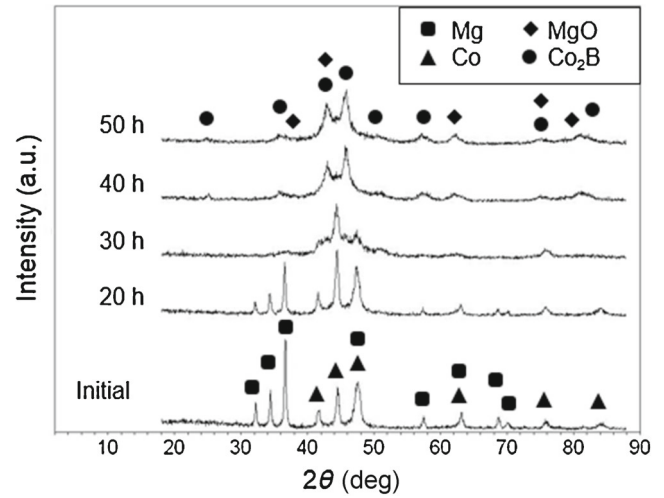


Figure 3. XRD graphs of the powders milled at 250 rpm and 30 : 1 BPR.

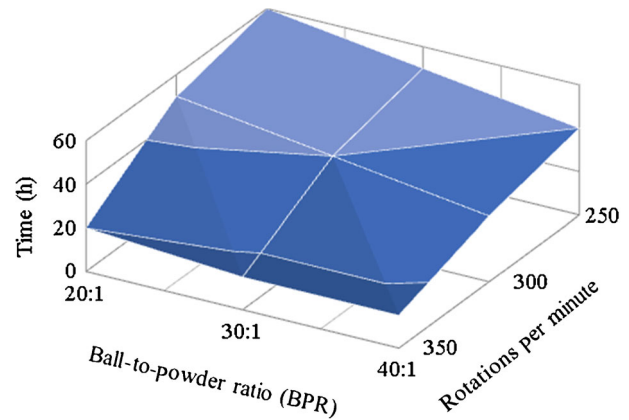


Figure 4. Reaction times of different rotational speeds and BPR.

between 9.28 and 34.60% and generally, the amount of powders adhering to the walls of vial and balls increased with the increase in the rotational speed. Figure 3 shows the phase conversions of powders in vial during the high-energy ball milling.

XRD graph in figure 3 shows that Mg decreased primarily in the starting material and MgO phase occurred gradually. This also specifies the reduction of B_2O_3 . In this way, reduced B and Co in the environment reacts and form a Co_2B . In MCS process, starting materials fracture by passing through the cycle of flattening, cold welding, fraction and re-flattening again and again with the mechanical energy formed during the milling and surface area of the materials increases with the decrease in grain size. The increase in surface area increases the reactivity and reactants, which become smaller with the increase in the milling time, enable the reaction to occur over time by entering interatomic spacings. This situation explains that starting materials reduced over time and the reaction occurred under room conditions.

The synthesizing period in MCS is according to parameters chosen in milling. The graphic in figure 4 shows the reaction

completion times in terms of different rotational speeds and BPR. It was seen from the graphic that the reaction time decreased as rotational speed and BPR ratio increased.

Mechanical energy applied to starting powders in the MCS enabled the desired reaction to occur in the environment gradually. However, proceed of milling even after completion of the reaction caused change in the structure. To understand this effect, experiments was carried out at 350 rpm rotational speed and 30 : 1 BPR were continued until 35 h and followed by XRD in certain periods. Figure 5 shows comparative XRD graphics of powders obtained for every 10 h during the milling.

The graphic shows that the reaction was completed within 15 h, crystal structure of the material deformed with proceed of milling process, and the structure progressed to amorphous. This result revealed the significance of milling time in the MCS. High mechanical energy applied to powder mixture in vial during the milling, deteriorated the crystal structure over time. Decreasing grain size and crystallite size over time caused slopes at crystal planes of the energy over

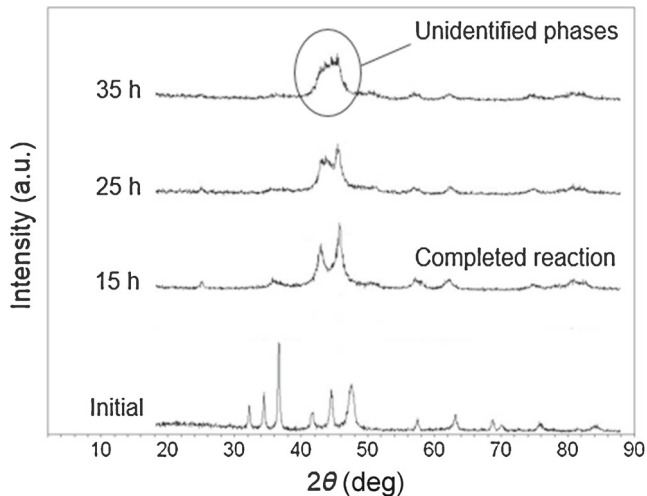


Figure 5. XRD graphic of powder mixtures obtained from synthesis experiments performed at 350 rpm and 30 : 1 BPR up to 35 h.

time. At XRD graphic, peaks observed at the end of 15 h shortened over time and the area under peak expanded. This change showed that crystallite size decreased and the structure became amorphous. In the study conducted by Avar and Özcan [41] with high-energy planetary ball mill, they revealed the effect of milling time on crystal structure. Similarly, they indicated that the crystal structure obtained deteriorated as milling time progressed and the structure became amorphous.

$\text{Co}_2\text{B} + \text{MgO}$ mixtures releasing in the milling processes were purified with acetic acid leach and powders obtained after leaching were dried in the vacuum environment. Figure 6 shows XRD analysis of Co_2B powders synthesized at different rotational speeds and 40 : 1 BPR, before and after leaching. XRD graphics clearly show that pure Co_2B phase was obtained by removing MgO phase from final mixture using AA leach. It is seen in the literature that hydrochloric acid (HCl) is mostly used for removing oxide phase released in synthesis studies conducted by using reductant with MCS [21,27,30,31,39]; furthermore, the AA leach gives successful results as well [23,42]. Because along with MgO, HCl is also a good dissolvent for Co_2B , AA has no dissolvent effect for Co_2B and was preferred for purification processes. The crystal structure of pure Co_2B nanocrystals were found to be tetragonal and the lattice parameters a and c were found to be 5.016 and 4.221 Å, respectively, from the PDF card of XRD graphic at figure 6.

Figure 7 shows SEM images taken to determine grain sizes and structures of synthesized Co_2B nanocrystals. It is seen from images that the obtained powders were irregular and coaxial. This situation was explained with the fact that the starting materials in ductile–ductile structure at the beginning of process were passed continuously through mechanisms of flattening cold welding, fraction, and again cold welding and reached ductile–brittle and brittle–brittle structure over time. As the mechanical energy applied to powders in milling was increased, ceramic phase transformations occurred more rapidly and thus, final powders irregularly and co-axially reached a stable equilibrium state [38].

Grain size distribution of all synthesized Co_2B nanocrystals was determined by using Image J 1.47v software based

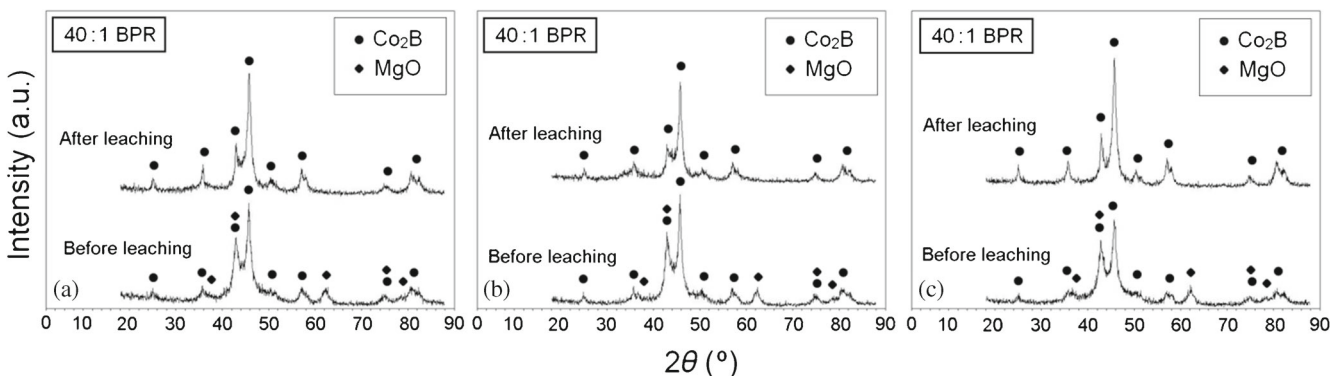


Figure 6. XRD graphics of Co_2B nanocrystals, synthesized at 40 : 1 BPR, before and after leaching: (a) 250, (b) 300 and (c) 350 rpm.

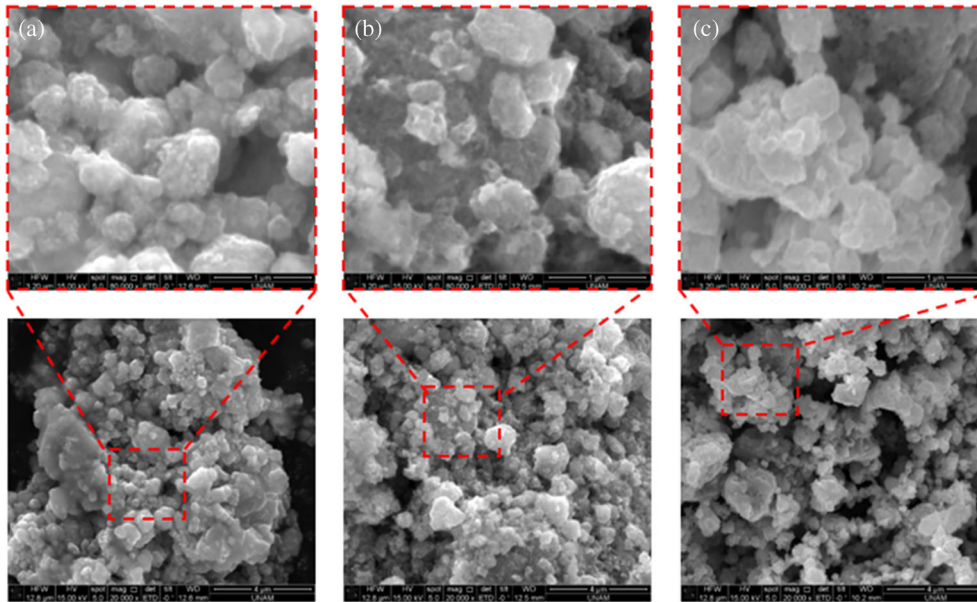


Figure 7. SEM images of Co_2B powders synthesized at 40 : 1 BPR: (a) 250, (b) 300 and (c) 350 rpm.

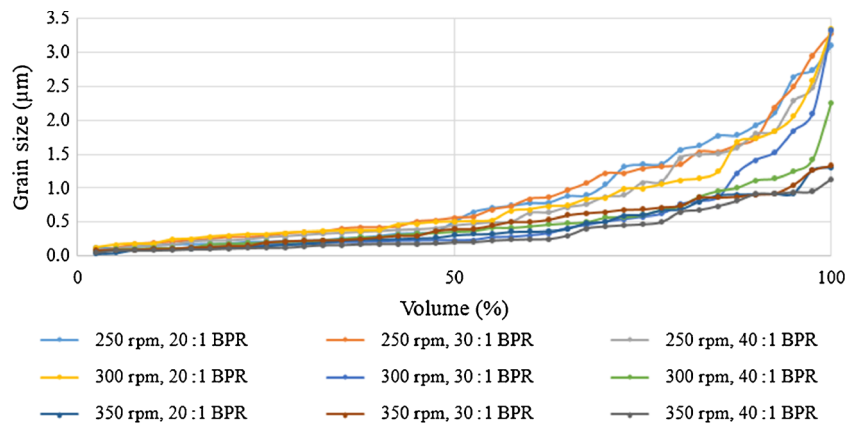


Figure 8. Grain size distributions of synthesized Co_2B powders.

on SEM images. From graphic, based on data obtained from SEM images and Image J 1.47v software shown in figure 8, it was determined that the products had a grain size of $\sim 4 \mu\text{m}$ and in almost all products $d(50)$ composed of particles smaller than 500 nm. Additionally, it was determined that products had wide distribution of grain size due to the nature of the MCS. Aggregation was observed in all the products. Aggregation seen on SEM images was associated with the vacuum applied to perform drying after purification process made by using the liquid method in addition to cold weld occurring during the milling.

Crystallite sizes of Co_2B nanocrystals synthesized at 40 : 1 BPR, after leaching were calculated by using the Scherrer formula given in equation (7). τ is crystallite size, K the constant depending on the crystal formation (0.89), λ the wavelength of X-ray (0.154 nm), β the full-width at half-maximum (FWHM) and θ the Bragg angle. According to FWHM and 2θ data of XRD graphics examined in Jade7.0 analysis software, crystallite sizes of products obtained at

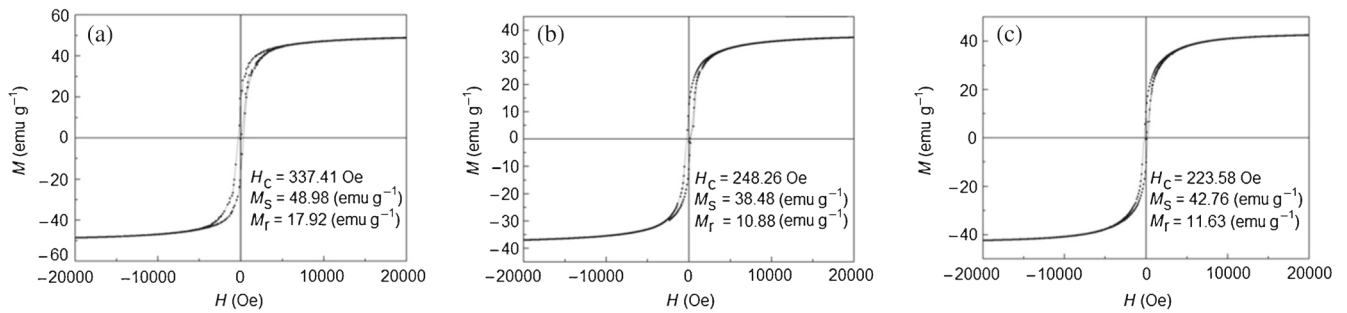
350 rpm rotational speed and 20 : 1–30 : 1–40 : 1 BPR were found as 9.84, 9.77 and 7.27 nm, respectively. Table 2 shows 2θ , FWHM and β -values taken from Jade7.0 software based on calculation and crystallite sizes obtained as a result of calculation

$$\tau = \frac{K\lambda}{\beta \cos \theta}. \quad (7)$$

While specific density analysis of the powders synthesized at 40 : 1 BPR and 250–300–350 rpm rotational speeds was performed to determine specific densities of Co_2B nanocrystals synthesized, BET analysis was performed to determine surface area. As a result of analyses, it was found that specific densities of Co_2B nanocrystals were 7.78, 7.75 and 7.61 g cm^{-3} and their surface areas were 21.14, 40.36 and 52.33 $\text{m}^2 \text{g}^{-1}$, respectively. The results showed that density of the product decreased and its surface area increased, BPR was kept constant and rotational speed was increased. This situation was interpreted and evaluated with the increase of

Table 2. 2θ , FWHM and β -values belonging to (100) peaks in XRD graphics of Co₂B nanocrystals synthesized at 40 : 1 BPR.

Rotation	Ball-to-powder			2θ (deg)	FWHM (deg)	β	Crystallite size (nm)
	ratio (BPR)	Time (h)					
350	20 : 1	40		45.821	0.868	0.015141778	9.84
	30 : 1	30		45.798	0.874	0.015246444	9.77
	40 : 1	15		45.765	1.175	0.020497222	7.27


Figure 9. Vibrating sample magnetization graphics of Co₂B nanocrystals synthesized at 40 : 1 BPR: (a) 250, (b) 300 and (c) 350 rpm.

nanoparticles in products synthesized in both circumstances (figures 7 and 8).

Also, the increase in the surface area and rotational speed, triggered the mechanisms of flattening, cold welding, fraction and re-flattening to occur more rapidly and also ceramic phases to form earlier. Early formation of ceramic phases caused the reduction of grain size more rapidly and increase in surface area is dependent on this.

Figure 9 illustrate the hysteresis loops of the Co₂B nanocrystals at 25°C. The coercivity (H_c), saturation magnetization (M_s) and remanent magnetization (M_r) values are also given in the figure. It was determined from measurements that all samples show ferromagnetic characteristics with a coercivity changing between 337 and 223 Oe and a saturation magnetization changing between 38 and 48 emu g⁻¹. Similarly, in their study, Kanomata *et al* [18] indicated that Co₂B particles synthesized with thermal method based on their elements had ferromagnetic property and a saturation magnetization of approximately 70 emu g⁻¹ under different pressure values. It was thought that the difference between values obtained from study conducted by Kanomata *et al* and values obtained as a result of the analysis was associated with the synthesis method and the reduced crystallite sizes of the samples.

In the MCS method, due to the reduced crystallite size and increased surface area of grinding surface, the ratio of the number of spins on the surface and at the volume of the crystallites has increased. This gives rise to the number of pinned spins because of the high surface anisotropy at the surface of the crystallites. Because of the pinning, their regularity of the surface spins causes a decrease in M_s value. From the literature, one can see that highly interacting magnetically ordered crystallites must show a M_r/M_s ratio with a value

of 0.5. But in this work, magnetic measurement shows that M_r/M_s ratio of the samples decreasing from 0.36 to 0.26 with the increase of the milling speed. This low M_r/M_s ratios indicates a low inter-particle interactions because of the magnetically disordered areas between the crystallites. This phenomenon was seen at the magnetic samples prepared with milling in literature and caused because of the amorphous areas that are induced by milling. With the increase at the milling speed and the decrease at the mean crystallites size, possibility of the amorphous areas is increased because of the high crystallite size distribution which is also a result of milling.

4. Conclusion

Pure Co₂B nanocrystals were successfully synthesized at different milling parameters in the planetary-type high-energy ball mill via the MCS method. Briefly, 40 : 1 BPR and 350 rpm were found as the most efficient parameters for synthesis of nanocrystals. Increases in BPR and rotating speed decreased the crystallite size of Co₂B nanocrystals gradually. All specimens exhibited ferromagnetic and hysteresis behaviours and saturation magnetization was between 35 and 50 emu g⁻¹. Co₂B nanocrystals crystallite size was between 7.27 and 9.84 nm, while their specific densities and surface areas varied between 7.61 and 7.78 g cm⁻³, and 21.14 and 52.33 m² g⁻¹, respectively.

Acknowledgement

We are very grateful to Eti Maden Works General Management for financial support and laboratory facilities usage.

References

- [1] Pratt J M and Swinden G 1969 *J. Chem. Soc. D* **22** 1321
- [2] Maybury P C, Mitchell R W and Hawthorn M F 1974 *J. Chem. Soc.: Chem. Commun.* **14** 534
- [3] Nitta Y, Imanaka T and Teranishi S 1980 *Bull. Chem. Soc. Jpn.* **53** 3154
- [4] Chen Y Z and Wu K J 1991 *Appl. Catal.* **78** 185
- [5] Glavee G N, Klabunde K J, Sorensen C M and Hadjapanayis G C 1993 *Langmuir* **9** 162
- [6] Petit C and Pileni M P 1997 *J. Magn. Magn. Mater.* **166** 82
- [7] Ma H Y, Li G Z, Zhang J P, Shen Q and Wang X 1998 *J. Dispers. Sci. Technol.* **19** 511
- [8] Wu C, Wu F, Bai Y, Yi B and Zhang H 2005 *Mater. Lett.* **59** 1748
- [9] Liu B H, Li Z P and Suda S 2006 *J. Alloys Compd.* **415** 288
- [10] Jeong S U, Cho E A, Nam S W, Oh I H, Jung U H and Kim S H 2007 *Int. J. Hydrogen Energy* **32** 1749
- [11] Ingersoll J C, Mani N, Thenmozhiyal J C and Muthaiah A 2007 *J. Power Sources* **173** 450
- [12] Walter J C, Andrew Z, Daniel M, Thornburg M and Revankar S 2008 *J. Power Sources* **179** 335
- [13] Liu B H and Li Q 2008 *Int. J. Hydrogen Energy* **33** 7385
- [14] Wang Y P, Wang Y J, Ren Q L, Li L, Jiao L F, Song D W, Liu G *et al* 2010 *Fuel Cells* **10** 132
- [15] Hongjing T, Qingjie G and Dongyan X 2010 *J. Power Sources* **195** 2136
- [16] Chuan W, Ying B, Dan-Xian L, Wu F, Pang M L and Yi B L 2011 *Catal. Today* **170** 33
- [17] Ozerova A M, Bulavchenko O A, Komova O V, Netskina O V, Zaikovskii V I, Odegova G V *et al* 2012 *Kinet. Catal.* **53** 511
- [18] Kanomata T, Ise Y, Kumagai N, Haga A, Kamishima K, Goto T, Kimura H M *et al* 1997 *J. Alloys Compd.* **259** L1
- [19] Choi S, Lapitan L D S, Cheng Y and Watanabe T 2014 *Adv. Powder Technol.* **25** 365
- [20] Iizumi K, Kudaka K, Maezawa D and Sasaki T 1999 *J. Ceram. Soc. Jpn.* **107** 491
- [21] Welham N J 2000 *J. Am. Ceram. Soc.* **83** 1290
- [22] Kudaka K, Iizumi K, Sasaki T and Okada S 2001 *J. Alloys Compd.* **315** 104
- [23] Kudaka K, Iizumi K, Izumi H and Sasaki T 2001 *J. Mater. Sci. Lett.* **20** 1619
- [24] Iizumi K, Sekiya C, Okadac S, Kudou K and Shishido T 2006 *J. Eur. Ceram. Soc.* **26** 635
- [25] Kim J W, Shim J H, Ahn J P, Cho Y W, Kim J H and Oh K H 2008 *Mater. Lett.* **62** 2461
- [26] Jiang X, Trunov M A, Schoenitz M, Dave R N and Dreizin E L 2009 *J. Alloys Compd.* **478** 246
- [27] Akgün B, Çamurlu H E, Topkaya Y and Sevinç N 2011 *Int. J. Refract. Met. Hard Mater.* **29** 601
- [28] Çamurlu H E 2011 *J. Alloys Compd.* **509** 5431
- [29] Balcı O, Ağaoğulları D, Duman İ and Öveçoğlu M L 2012 *Ceram. Int.* **38** 2201
- [30] Ağaoğulları D, Duman İ and Öveçoğlu M L 2012 *Ceram. Int.* **38** 6203
- [31] Balcı Ö, Ağaoğulları D, Duman İ and Öveçoğlu M L 2012 *Powder Technol.* **225** 136
- [32] Shao J, Xiao X, Fan X, Chen L, Zhu H, Yu S *et al* 2013 *Mater. Lett.* **109** 203
- [33] Bahrami-Karkevandi M, Ebrahimi-Kahrizsangi R and Nasiri-Tabrizi B 2014 *Int. J. Refract. Met. Hard Mater.* **46** 117
- [34] Torabi O, Naghibi S, Golabgir M H, Tajizadegan H and Jamshidi A 2015 *Ceram. Int.* **41** 5362
- [35] Jafari M, Tajizadegan H, Golabgir M H, Chami A and Torabi O 2015 *Int. J. Refract. Met. Hard Mater.* **50** 86
- [36] Torabi O, Ebrahimi-Kahrizsangi R, Golabgir M H, Tajizadegan H and Jamshidi A 2015 *Int. J. Refract. Met. Hard Mater.* **48** 102
- [37] Wang Y D, Guang X Y and Mu P 2012 *Chin. Sci. Bull.* **57** 4225
- [38] Suryanarayana C 2004 *Mechanical alloying and milling* (New York: Marcel Dekker)
- [39] Önder O 2009 Synthesis of lithium borides by mechanochemical process *Master Thesis* (Ankara: Middle East Technical University)
- [40] Can M M, Özcan Ş, Ceylan A and Fırat T 2010 *Mater. Sci. Eng. B* **172** 72
- [41] Avar B and Özcan S 2015 *J. Alloys Compd.* **650** 53
- [42] Şimşek T 2014 Investigation of the zirconium diboride nanocrystal coated different materials mechanic and mechaniability properties *PhD Thesis* (Ankara: Gazi University)